Research Article
Cancer

JOURNAL
OF HEPATOLOGY

Dynamics and predicted drug response of a gene network linking dedifferentiation with beta-catenin dysfunction in hepatocellular carcinoma

Graphical abstract

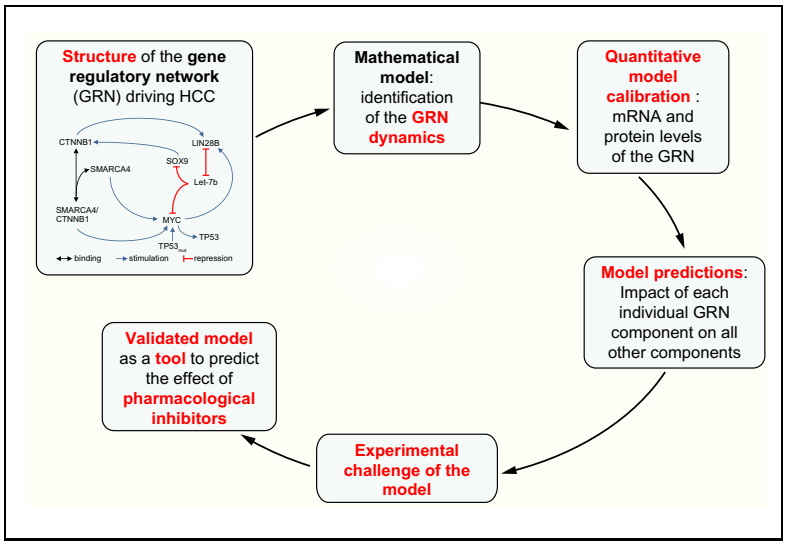

Highlights

- We identified a gene regulatory network (GRN) involved in a subset of hepatocellular carcinomas.
- Expression of GRN members and targets correlates with proliferation and prognosis.
- A quantitative mathematical model of the GRN revealed the network dynamics.
- This model is a potential tool to assess the impact of pharmacological inhibitors.

Authors

Claude Gérard, Mickaël Di-Luoffo, Léolo Gonay, ..., Jens U. Marquardt, Jessica Zucman-Rossi, Frédéric P. Lemaigre

Correspondence

frederic.lemaigre@uclouvain.be
(F.P. Lemaigre)

Lay summary

Hepatocellular carcinoma (HCC) is a heterogeneous disease driven by the concomitant deregulation of several genes functionally organized as networks. Here, we identified a gene regulatory network involved in a subset of HCCs. This subset is characterized by increased proliferation and poor prognosis. We developed a mathematical model which uncovers the dynamics of the network and allows us to predict the impact of a therapeutic agent, not only on its specific target but on all the genes belonging to the network.

http://dx.doi.org/10.1016/j.jhep.2019.03.024
 J. Hepatol. 2019, 71, 323–332

Research Article
Cancer

JOURNAL OF HEPATOLOGY

Dynamics and predicted drug response of a gene network linking dedifferentiation with beta-catenin dysfunction in hepatocellular carcinoma

Claude Gérard[1], Mickaël Di-Luoffo[1], Léolo Gonay[1,2], Stefano Caruso[3,4], Gabrielle Couchy[3,4], Axelle Loriot[1], Darko Castven[5], Junyan Tao[6], Katarzyna Konobrocka[1], Sabine Cordi[1], Satdarshan P. Monga[6], Emmanuel Hanert[2], Jens U. Marquardt[5], Jessica Zucman-Rossi[3,4], Frédéric P. Lemaigre[1,*]

[1]*de Duve Institute, Université catholique de Louvain, Brussels, Belgium;* [2]*Earth and Life Institute, Université catholique de Louvain, Louvain-la-Neuve, Belgium;* [3]*Centre de Recherche des Cordeliers, Sorbonne Universités, Inserm, UMRS-1138, F-75006 Paris, France;* [4]*Functional Genomics of Solid Tumors, USPC, Université Paris Descartes, Université Paris Diderot, Université Paris 13, Labex Immuno-Oncology, équipe labellisée Ligue Contre le Cancer, F-75000 Paris, France;* [5]*Department of Medicine I, Johannes Gutenberg University, Mainz, Germany;* [6]*Department of Pathology, Medicine and the Pittsburgh Liver Research Center, University of Pittsburgh, School of Medicine and University of Pittsburgh Medical Center, Pittsburgh, PA, USA*

Background & Aims: Alterations of individual genes variably affect the development of hepatocellular carcinoma (HCC). Thus, we aimed to characterize the function of tumor-promoting genes in the context of gene regulatory networks (GRNs).

Methods: Using data from The Cancer Genome Atlas, from the LIRI-JP (Liver Cancer – RIKEN, JP project), and from our transcriptomic, transfection and mouse transgenic experiments, we identify a GRN which functionally links LIN28B-dependent dedifferentiation with dysfunction of β-catenin (*CTNNB1*). We further generated and validated a quantitative mathematical model of the GRN using human cell lines and *in vivo* expression data.

Results: We found that LIN28B and CTNNB1 form a GRN with SMARCA4, Let-7b (*MIRLET7B*), SOX9, TP53 and MYC. GRN functionality is detected in HCC and gastrointestinal cancers, but not in other cancer types. GRN status negatively correlates with HCC prognosis, and positively correlates with hyperproliferation, dedifferentiation and HGF/MET pathway activation, suggesting that it contributes to a transcriptomic profile typical of the proliferative class of HCC. The mathematical model predicts how the expression of GRN components changes when the expression of another GRN member varies or is inhibited by a pharmacological drug. The dynamics of GRN component expression reveal distinct cell states that can switch reversibly in normal conditions, and irreversibly in HCC. The mathematical model is available via a web-based tool which can evaluate the GRN status of HCC samples and predict the impact of therapeutic agents on the GRN.

Conclusions: We conclude that identification and modelling of the GRN provide insights into the prognosis of HCC and the mechanisms by which tumor-promoting genes impact on HCC development.

Lay summary: Hepatocellular carcinoma (HCC) is a heterogeneous disease driven by the concomitant deregulation of several genes functionally organized as networks. Here, we identified a gene regulatory network involved in a subset of HCCs. This subset is characterized by increased proliferation and poor prognosis. We developed a mathematical model which uncovers the dynamics of the network and allows us to predict the impact of a therapeutic agent, not only on its specific target but on all the genes belonging to the network.

Introduction

Various etiologies are associated with HCC, leading to heterogeneity in clinical outcome, histology, transcriptomic profile and mutational spectrum.[1–5] Such heterogeneity causes a variable response to therapeutic agents, as in mouse models with *Ctnnb1*-induced HCCs which show heterogeneous sensitivity to CTNNB1 inhibitors.[6] Thus, designing novel therapeutic strategies against HCC requires the identification of inhibitors of individual tumor-promoting genes and also the characterization of the molecular networks in which those genes exert their functions.

Dedifferentiation of hepatic cells contributes to HCC progression.[7–9] In this context, poorly differentiated HCC develop as a result of forced induction of LIN28B, an RNA-binding protein which is repressed during normal hepatic cell differentiation. LIN28B is re-expressed in a subset of human HCCs characterized by high serum levels of α-fetoprotein,[10,11] thereby associating dedifferentiation, HCC progression and LIN28B expression.[12] In parallel, *CTNNB1* is one of the most frequently mutated genes in HCC.[13] Therefore, we explore the possibility that HCC progression depends on a gene regulatory network (GRN)

Keywords: Hepatocellular carcinoma; Mathematical model; Gene regulatory network; HGF/MET pathway; Principal component analysis; MicroRNA; LIN28B; CTNNB1; Personalized medicine.
Received 16 August 2018; received in revised form 15 March 2019; accepted 21 March 2019; available online 4 April 2019

* Corresponding author. Address: de Duve Institute, Université catholique de Louvain, Avenue Hippocrate 75 (B1-75.03), 1200 Brussels, Belgium. Tel.: +32 2 764 7583 (direct)/+32 2 764 7550 (secretariat); fax: +32 2 764 7573.
E-mail address: frederic.lemaigre@uclouvain.be (F.P. Lemaigre).

linking LIN28B-dependent dedifferentiation with CTNNB1 dysfunction.

Several approaches can be used to identify GRNs.[14] Here, we selected a method which captures the biological logic of gene networks. The identification of the network is literature-based. The number of interacting components in the network is limited but perfectly compatible with the characterization of the network's dynamics by our mathematical modelling approach.[15,16] We identified an HCC-promoting GRN comprising several members connecting LIN28B with CTNNB1 via Let-7b (*MIRLET7B*), MYC, SMARCA4 (also called BRG1), TP53 and SOX9. We further investigated the system-level dynamics of the GRN using a quantitative mathematical model, which was calibrated and validated using mRNA and protein expression data from HCC cell lines, primary HCC cells, patient databanks and mouse models.

Materials and methods

Data normalization and statistical analysis

Data normalization is described in the supplementary information. Measured data are means ± SD. Significance was assessed by Student's *t* test (*p* value). For RNA sequencing data of the HCC cohort from The Cancer Genome Atlas (TCGA), we calculated the adjusted *p* value using a Benjamini-Hochberg correction (p^* value) on the entire transcriptome.

RNA sequencing and miRNA sequencing

Data were from TCGA (http://firebrowse.org/), and from LIRI-JP (RIKEN) of the International Cancer Genome Consortium (ICGC; https://dcc.icgc.org/projects/LIRI-JP). For the TCGA cohort, we converted the "scaled_estimate" in the "illuminahiseq_rnaseqv2_unc_edu_Level_3_RSEM_genes" file into TPM by multiplying by 10^6.

Plasmids and microRNAs

pCDNA3.1, pcDNA3-MYC, pCl-neo β-Catenin (CTNNB1^{S33Y}), pBABE-BRG1 were from Thermo Fisher Scientific (Waltham, MA, USA), Wafik El-Deiry (Addgene plasmid # 16011), Bert Vogelstein (Addgene plasmid # 16519) and Robert Kingston (Addgene plasmid # 1959) respectively. The miR mimic control (MIMAT0000039: UCACAACCUCCUAGAAAGAGUAGA) and miR mimic hsa-let-7b: hsa-let-7b-5p (MIMAT0000063: UGAGGUAGUAGGUUGUGUGGUU), hsa-let-7b-3p (MIMAT0004482: CUAUACAACCUACUGCCUUCCC) were from Dharmacon (Lafayette, CO, USA).

Cell culture

Human Huh7, HepG2, Hep3B cell lines and primary human HCC cells HCC31[17] were grown in DMEM (Lonza, Leusden, Netherlands), 10% fetal bovine serum (5% for HCC31; Merck, Darmstadt Germany), L-Glutamine (2 mM) (Thermo Fisher Scientific), Penicillin-Streptomycin (50 U/ml and 50 μg/ml) (Gibco™, Waltham, MA, USA) and Amphotericin B (Gibco™) (2.5 μg/ml). Cells were grown in 60 mm dishes and transfected with 3 μg plasmid and 120 nM miRmimic, using jetPRIME® (Polyplus-Transfection, Illkirch-Graffenstaden, France) for 48, 72 or 96 h, in at least 3 independent experiments. DNA was transfected 24 h after plating the cells. For LIN28 inhibition, Huh7 and HCC31 cells were grown in the presence of 120 μM (*N*-Methyl-*N*-[3-(3-methyl-1,2,4-triazolo[4,3-*b*]pyridazin-6-yl) phenyl]acetamide) for 6 days; the medium with inhibitor was changed every day.

Western blotting

Protocol and antibodies are described in the supplementary information.

RNA extraction and analysis

Total RNA was isolated from Huh7 cells using Trizol (#1029602, Invitrogen, Life technologies). cDNA synthesis was performed with MMLV reverse transcriptase (#28025-13, Invitrogen, Life technologies) according to manufacturer's protocol. MicroRNA expression (Let-7a and Let-7b) was quantified by reverse transcription quantitative PCR (RT-qPCR) using Kapa SYBR Fast 2X Universal Master Mix (#KK4601, Sopachem, Ochten, Netherlands). Specific stem-loop primers were used for reverse transcription, and RT-qPCR was performed using a specific forward primer and a common universal reverse primer. *Let-7a* Fwd/Rev: ACACTCCAGCTGGGTGAGGTAGTAGGTTG/CTCAACTGGTGTCGTGGAGTCGGCAATTCAGTTGAGACTATACA; *Let-7b* Fwd/Rev: ACACTCCAGCTGGGTGAGGTAGTAGGTTGT/CTCAACTGGTGTCGTGGAGTCGGCAATTCAGTTGAGAACCACAC; *ACTB* Fwd/Rev: TCCTGAGCGCAAGTACTCTGT/CTGATCCACATCTGCTGGAAG. Each ΔCt between the measured transcripts and the housekeeping genes was normalized to their control conditions using the $2^{-\Delta\Delta Ct}$ method.

For further details regarding the materials used, please refer to the CTAT table and supplementary information.

Results

Identification of a gene regulatory network driving hepatocellular carcinoma

We selected an approach in which GRN members meet stringent functional criteria. First, their role in tumor promotion must be validated by animal experimentation and/or high-throughput sequencing data from patients. Second, GRN members must be connected by direct or indirect functional links characterized by protein-protein and protein-DNA interactions, or epistatic relationship identified in loss- and gain- of function analyses. By combining data from the literature, we first reconstituted a GRN comprising 7 cross-regulating components: the miRNA *Let-7b*, the RNA-binding protein LIN28B, the ATP-dependent helicase SMARCA4, and the transcription factors SOX9, MYC, CTNNB1 and TP53 (Fig. 1A; supplementary information, section 1). When interactions have been identified in non-hepatic cells, we verified whether they also occurred in cultured HCC cell lines (see below).

Data from TCGA (Fig. 1A) showed that expression of *Let-7b* is reduced in HCC compared to adjacent non-tumor tissue. This is consistent with the concomitant overexpression of LIN28B, a repressor of *Let-7b*. All other GRN components, except MYC, were increased in HCC. Further, a principal component analysis (PCA), which considers only the expression of the 7 GRN components in 50 non-tumor controls and 368 HCCs revealed that non-tumor tissue and HCC tumors clustered separately (Fig. 1B and Fig. S1A). In addition, we clustered the HCC cohort in 2 groups of 100 samples based on the low versus high expression levels of each GRN component. This analysis showed that, except for *Let-7b*, high expression of a component is associated with high expression of the other GRN components. (Fig. S2; supplementary information, Section 2).

PCA investigating multiple targets of the GRN components (Table S1) identified separate clusters for non-tumor tissue and HCC tumors, indicating that the components of the GRN

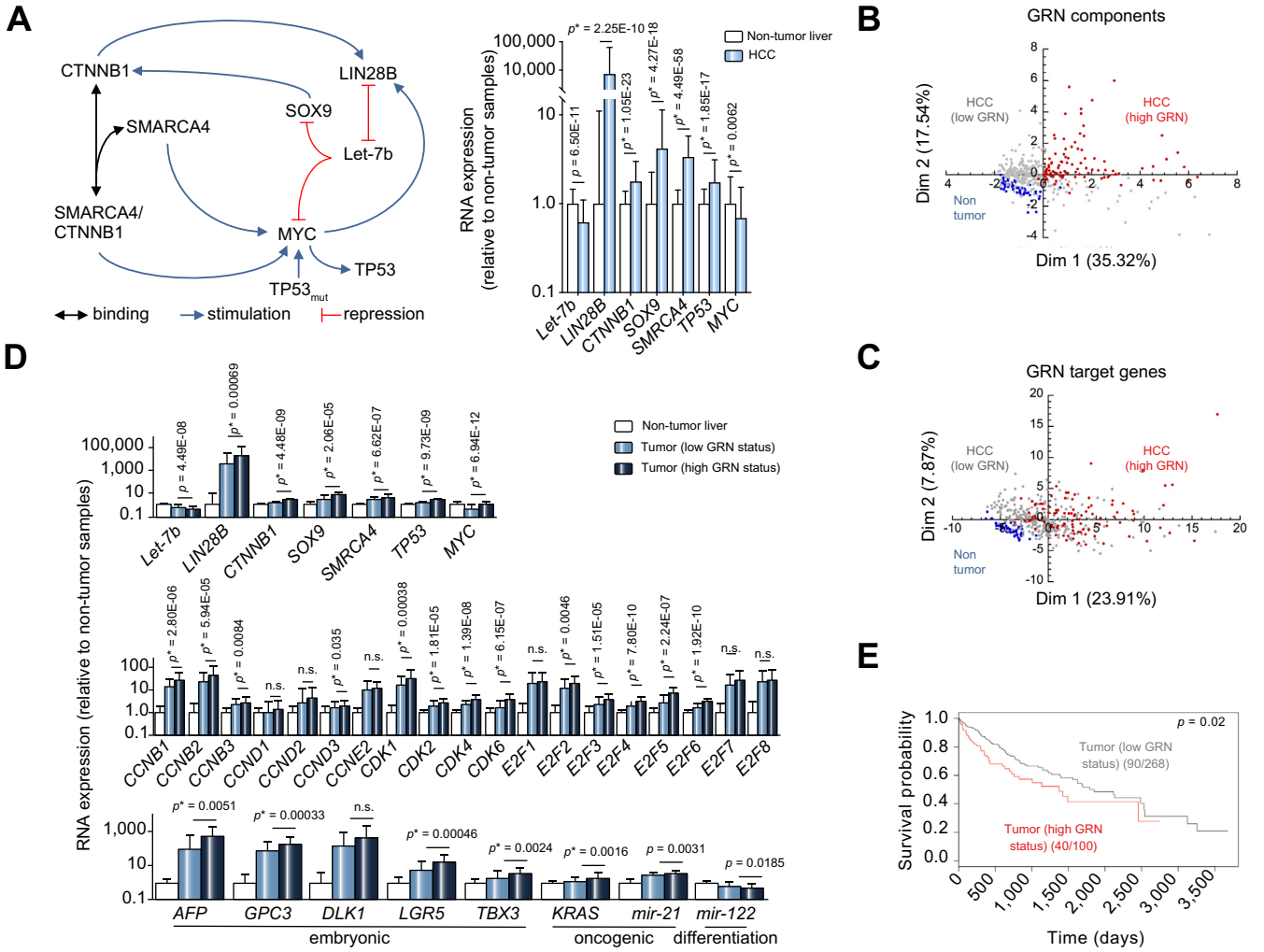

Fig. 1. Identification of a GRN involved in HCC. (A) Structure of the GRN (left), and RNA levels of GRN components in non-tumor tissue (n = 50) and HCC tumors (n = 368) from the HCC cohort in TCGA (right). (B) PCA plots based on the expression of the GRN components, and (C) on selected GRN targets (Table S1) in control and HCC samples. (D) Tumors were ranked according to low or high GRN status. Expression of the GRN components correlated well with high GRN status (top); and with expression of proliferation (middle), embryonic and oncogenic markers (bottom), and with lowest levels of the differentiation marker miR-122 (bottom). (E) Kaplan-Meier curves (overall survival) showed that patients with high GRN status (median time = 1,372 days, 40 deceased patients amongst 100) exhibited a lower survival probability than patients with low GRN status (median time = 1,852 days, 90 dead patients amongst 268) (Wilcoxon test, $p = 0.02$). p = p value (Student's t test); p^* = p value (Student's t test with Benjamini-Hochberg correction on the entire transcriptome). GRN, gene regulatory network; HCC, hepatocellular carcinoma; PCA, principal component analysis; TCGA, The Cancer Genome Atlas. (This figure appears in colour on the web.)

were not only dysregulated in HCC but also that they were actively controlling their targets (Fig. 1C and Fig. S1B). Therefore, we considered that concomitant overexpression of the GRN components LIN28B, SMARCA4, SOX9, CTNNB1 and TP53, and downregulation of Let-7b is indicative of GRN activity.

Out of the 368 HCCs from the TCGA cohort whose GRN component expression had been analyzed by PCA we selected the 150 samples with the highest Dimension 1 to which *CTNNB1*, *SMARCA4*, *SOX9, MYC* and *TP53* expression contribute the most, and out of the latter we selected the 100 samples with highest Dimension 2 to which *LIN28B* and *Let-7b* contribute the most (Fig. S1A and red dots in Fig. 1B). These 100 samples were defined hereafter as displaying high GRN status and were compared with the other 268 tumors, which were defined as low GRN status, and with non-tumor liver tissue. The expression of the GRN components differed significantly between the tumors with low and high GRN status (Fig. 1D). Moreover, the samples with high GRN status displayed the highest expression of proliferation, embryonic and oncogenic markers, and the lowest levels of differentiation markers (Fig. 1D).

HCCs are divided in proliferative and non-proliferative classes.[13] GRN status, defined as above, correlated with increased MET signaling, a pathway whose activation characterizes a subset of the proliferative HCC class.[18] Indeed, HCCs with low or high GRN status clustered separately from the non-tumor samples in a PCA plot when considering the expression of 110 HGF/MET target genes (Fig. 2A). In addition, the 100 tumors with highest HGF/MET target gene expression displayed increased expression of *CTNNB1*, *SOX9*, *SMARCA4*, *MYC* and *TP53* compared to the other 268 tumors (Fig. 2B).

Earlier transcriptomic analyses classified patients with HCC into 6 subgroups, G1 to G6.[19] PCA analysis using 216 randomly selected genes that are differentially expressed in G1 to G6, revealed that tumors from the TCGA cohort with high GRN status cluster the farthest from the non-tumor tissue (Fig. 2C). Among the 216 genes differentially expressed between the G1

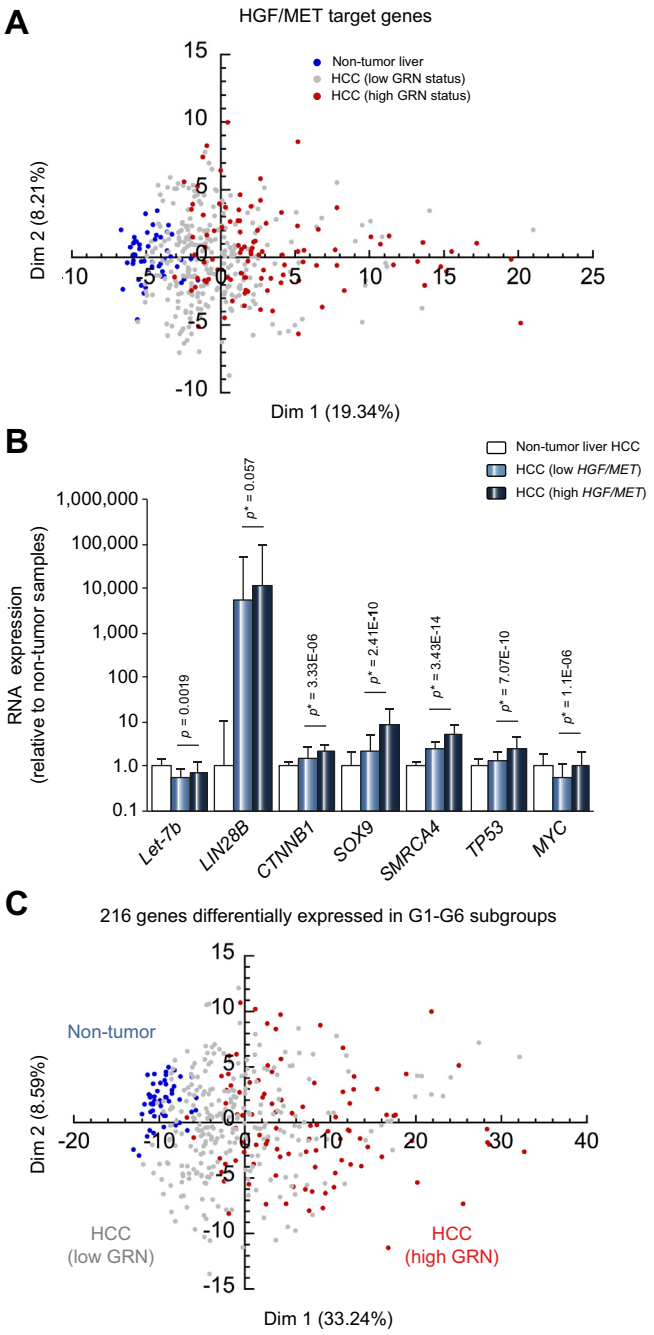

Fig. 2. The gene regulatory network promotes a proliferative HCC phenotype. (A) Non-tumor samples (blue; n = 50) and HCCs (n = 368) cluster separately in a PCA analysis based on the expression of 110 HGF/MET target genes (Table 1 in Ref. 18). (B) Expression of GRN components in non-tumor samples (blue, n = 50) and in HCC with low (grey; n = 268) or high HGF/MET target expression (red; n = 100). 100 tumor samples with high HGF/MET signaling were selected by PCA analysis based on the expression levels of 110 HGF/MET target genes (panel A). (C) Clustering of normal (blue) *vs.* HCC with low (grey) and high GRN status (red) in a PCA analysis based on the expression of 216 differentially expressed genes of the 6-group HCC classification. (B) Data are means ± SD. GRN, gene regulatory network; HCC, hepatocellular carcinoma; PCA, principal component analysis. *p* and *p** calculated as in Fig. 1. (This figure appears in colour on the web.)

to G6 subgroups, the 50 genes that contribute the most to the Dimension 1 in the PCA plot were all upregulated in G1, G2 and G3 and were mainly involved in cell proliferation (Table S2), supporting the idea that GRN functionality may contribute to confer a transcriptomic profile typical of the HCC proliferation class.

We also investigated whether GRN status correlated with prognosis. The survival probability was lower in the 100 patients with HCC and a high GRN status than in the 268 patients with HCC and a low GRN status (Fig. 1E). When performing the same analysis with individual components of the GRN, the expression of *Let-7b*, *MYC* and *TP53* did not correlate with survival, while expression of *CTNNB1*, *SOX9*, *SMARCA4* and *LIN28B* were inversely correlated with survival (Fig. S3). Therefore, the status of the GRN is a good marker of prognosis.

To determine if the characteristics of HCC with high GRN status are valid for a distinct patient cohort, we analyzed the GRN in the LIRI-JP (Riken) cohort from the ICGC. As in the TCGA cohort, the HCC with low or high GRN status clustered separately (Fig. 3A). The GRN is also functional in LIRI-JP since HCC with high GRN status overexpress the GRN target genes (Fig. 3A). HCC with high GRN status also overexpress proliferation markers and the HGF/MET target genes (Fig. 3B-C), and negatively correlate with prognosis (Fig. 3D).

In conclusion, we have identified a GRN of functionally interacting partners which are misexpressed in HCC. The status of the GRN, characterized by consistent and concomitant misexpression of its components and targets, correlates with proliferation, dedifferentiation and prognosis.

Mathematical model of the GRN

To develop a tool that determines how variation of an individual GRN component affects the expression of all the others, we built a quantitative mathematical model, using a set of 20 kinetic equations describing the expression of each network component (mRNA and protein) as a function of time (supplementary information, sections 3–4). We quantitatively calibrated the model using the mRNA levels of all GRN components available in TCGA and in a dataset from 34 human HCC cell lines[20] (Fig. S4A-C). Two sets of parameter values and initial conditions were determined for normal tissues on one hand, and for HCC tumors and cell lines on the other hand (Tables S3-7).

To quantitatively calibrate the model with protein expression values we transiently overexpressed GRN components in cultured HCC cell lines. These experiments validated in HCC the cross-regulating pairs of the GRN which had originally been identified in non-hepatic tumors. Indeed, overexpression of MYC in HepG2 or Huh7 cells stimulated TP53 and *LIN28B* expression, thereby validating in HCC the MYC → *TP53* and MYC → *LIN28B* interactions (Fig. 4A and Fig. S5A). Similarly, overexpression of constitutively active $CTNNB1^{S33Y}$ and of SMARCA4 in HepG2 or Huh7 cells validated the CTNNB1 → *LIN28B* and CTNNB1 → *MYC* and SMARCA4 → *MYC* interactions in HCC (Fig. 4B and Fig. S5B-C). Finally, transient transfection of *Let-7b-5p* mimic RNA repressed LIN28B, MYC and SOX9, confirming the regulatory links in the GRN (Fig. 4C).

The duration of the transient transfections in Fig. 4 (48 h, 72 h, 96 h) reflected the minimal time-lapse required to monitor a significant change in TP53, LIN28B, MYC or SOX9 protein levels following overexpression of their respective stimulator or repressor. Therefore, both the level of protein induction and the timing required to observe a significant change in protein level were used to further calibrate the mathematical model, while maintaining the quantitative calibration of all mRNA expression levels. We then simulated the transient transfection conditions by increasing the transcription rate constants of

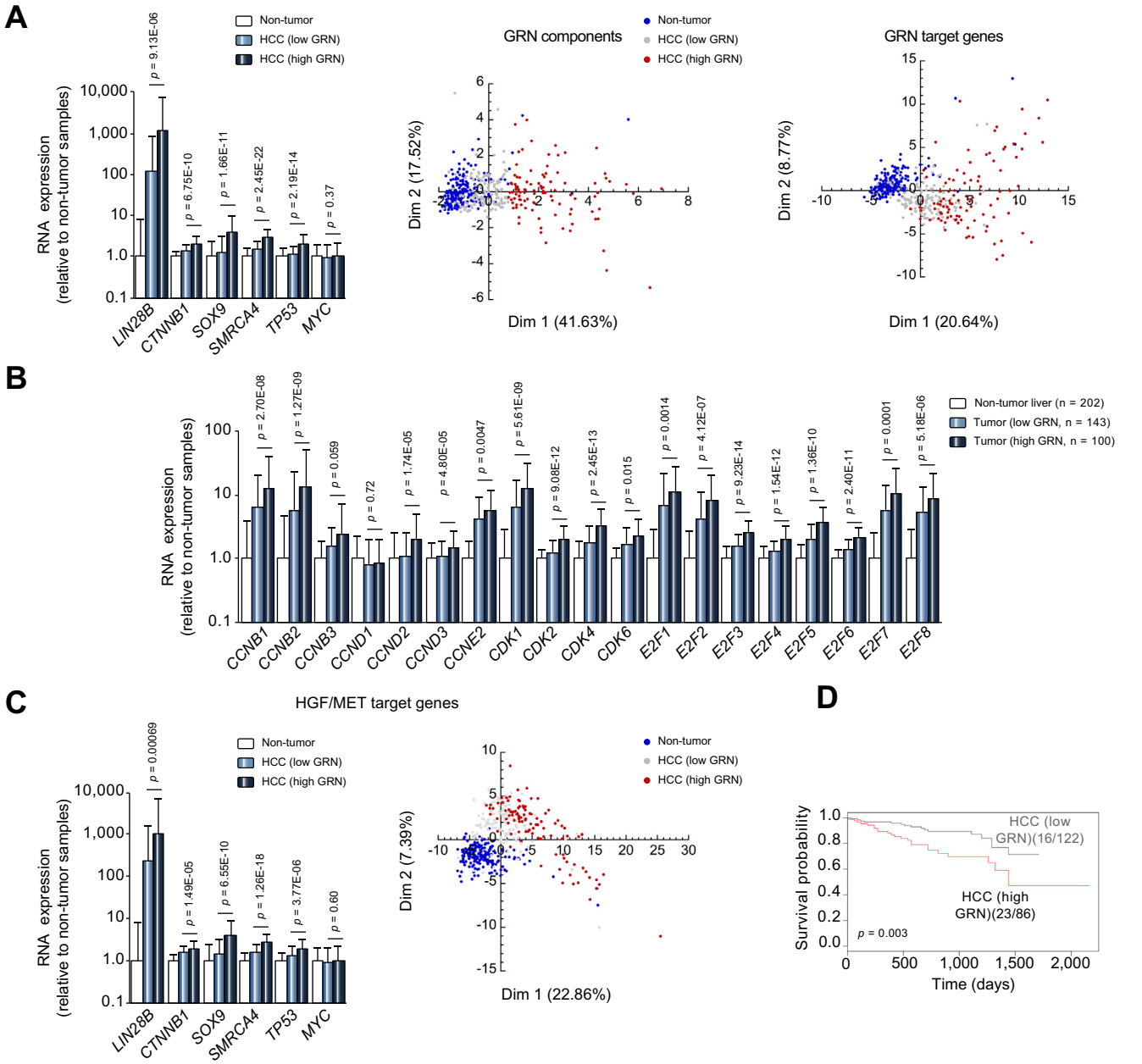

Fig. 3. Validation of the GRN in the LIRI-JP HCC cohort. (A, left) mRNA levels of GRN components in non-tumor tissue (n = 202) and HCC tumors (n = 243) from the HCC cohort (LIRI-JP) in ICGC. (A, middle) PCA plots based on the expression of the GRN components, and (A, right) on GRN targets (listed in Table S1) in control (blue), HCC low (grey) or high GRN status (red). (B) Expression of the GRN components correlated well with expression of proliferation markers. (C, left) Expression of GRN components in non-tumor samples (blue, n = 202) and in HCC with low (grey; n = 142) or high HGF/MET target expression (red; n = 100). (C, right) Non-tumor samples (blue; n = 202), HCC low GRN (grey; n = 142) and HCC high GRN status (red; n = 100) cluster separately in a PCA analysis based on the expression of 110 HGF/MET target genes. Data are means ± SD; *p* and *p** calculated as in Fig. 1. (D) Kaplan-Meier curves (overall survival) showed that patients with high GRN status (23 deceased patients amongst 86) exhibited a lower survival probability than patients with low GRN status (16 dead patients amongst 122) (Wilcoxon test, $p = 0.003$). GRN, gene regulatory network; HCC, hepatocellular carcinoma; ICGC, International Cancer Genome Consortium; PCA, principal component analysis; TCGA, The Cancer Genome Atlas. (This figure appears in colour on the web.)

MYC, CTNNB1 or *Let-7b*, starting at t = 0 h (Fig. 4A-C, right). The results showed that simulating a 10-fold increase in MYC, which mimics the observed 10-fold increase in transfected MYC protein, predicted a ~ 2-fold increase in LIN28B and TP53 after 72 h; this predicted increase in LIN28B and TP53 matched closely the measured values (compare white and blue bars in Fig. 4A). Similarly, simulating an 8-fold increase in $CTNNB1^{S33Y}$ predicted a ~ 3- and 11-fold induction of LIN28B and MYC after 48 h; these inductions again matched closely the measured 4- and 9-fold induction of LIN28B and MYC, following an 8-fold increase in transfected $CTNNB1^{S33Y}$ (Fig. 4B). Moreover, following a simulated 8-fold induction of *Let-7b* the model reproduced quantitatively the experimentally measured impact of *Let-7b* induction on LIN28B, MYC, and SOX9 (Fig. 4C). Finally, Let-7b induction in Huh7 cells did not affect *CTNNB1* expression, which fitted with the simulation (Fig. 4C). We concluded that the mathematical model faithfully recapitulates the expression of GRN components.

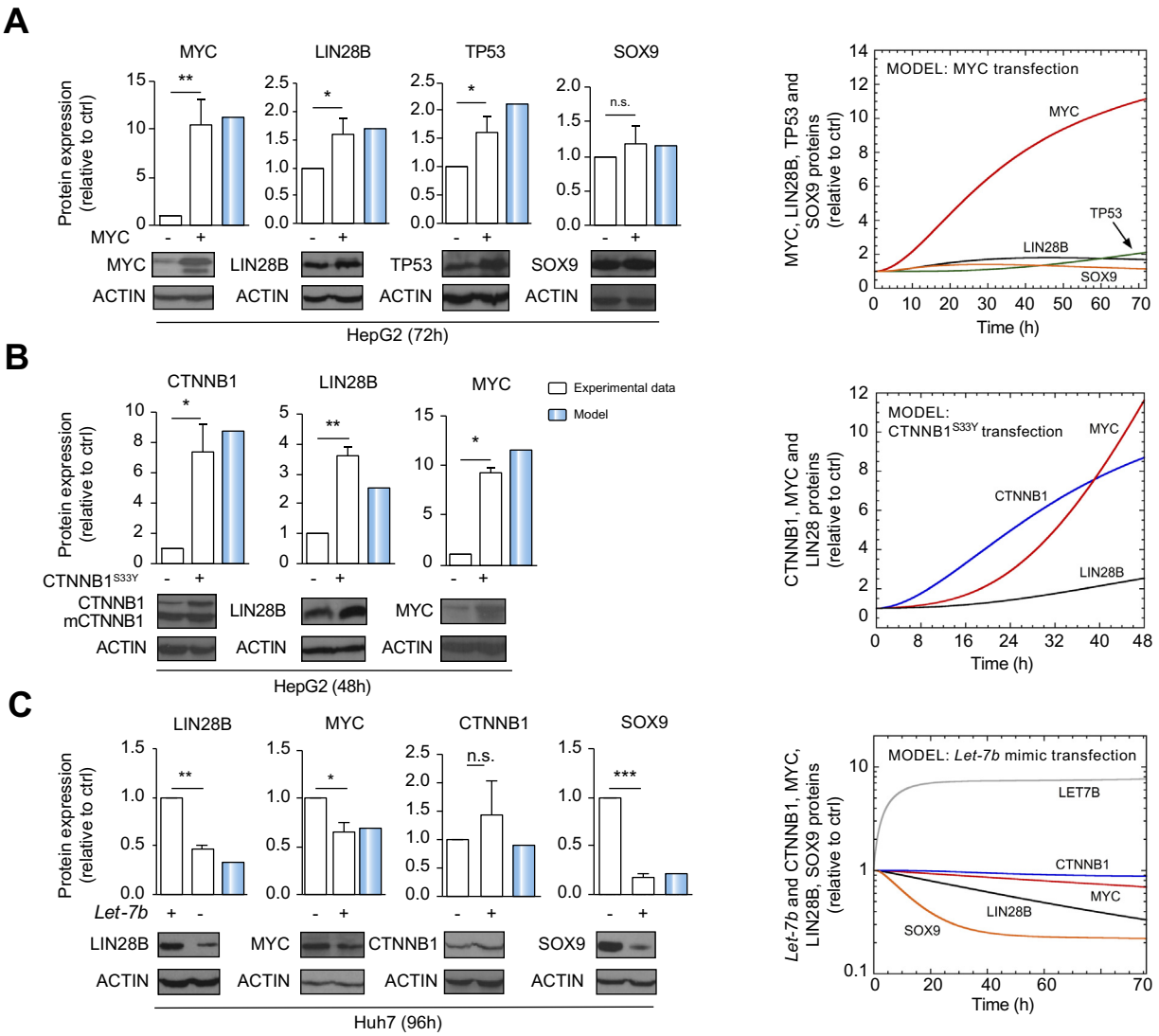

Fig. 4. Calibration of the mathematical model on protein expression in human HCC cell lines. (A) Expression of MYC, LIN28B, TP53 and SOX9 protein following MYC overexpression in HepG2 cells. (B) Expression of CTNNB1, LIN28B and MYC protein following CTNNB1^{S33Y} overexpression in HepG2 cells. mCTNNB1 corresponds to endogenous mutant CTNNB1 resulting from inframe deletion of exon 3. (C) Expression of LIN28B, MYC, CTNNB1 and SOX9 in the presence of *Let-7b-5p* mimic RNA in Huh7 cells. Data in bar graphs are means ± SD, n ≥ 3. $^{*}p < 0.05$; $^{**}p < 0.01$ and $^{***}p < 0.001$ (Student's *t* test). Blue bars correspond to protein levels calculated in the mathematical model with (A) overexpression of MYC, (B) overexpression of CTNNB1^{S33Y} and (C) overexpression of *Let-7b*. The right panels in A-C show the simulated temporal evolution, with the appropriate time scale, of the GRN proteins following MYC, CTNNB1^{S33Y}, or *Let-7b* mimic transfection. See supplementary information for parameter values and initial conditions. GRN, gene regulatory network; HCC, hepatocellular carcinoma. (This figure appears in colour on the web.)

Validation of the mathematical model in mouse and human

To validate the model, we challenged it by predicting the impact of a stabilizing CTNNB1 mutation on *LIN28B* and *Let-7b* expression and compared the prediction with values from TCGA. To this end we first partitioned the HCC samples of the TCGA database into 2 cohorts characterized by the presence or absence of a stabilizing CTNNB1 mutation, the most frequent *CTNNB1* mutations being missense mutations in exon 3. This revealed that *CTNNB1* mRNA levels were higher in the presence of a mutation (Fig. 5A). Therefore, to simulate CTNNB1 stabilization in the model we increased the *CTNNB1* mRNA synthesis rate, increased the activation rate of the inactive (complexed) CTNNB1 form, and decreased the inactivation rate of the active (stabilized) form. Under these conditions, when *CTNNB1* mRNA values from the mutated and non-mutated samples were introduced into the model (Fig. 5A, blue bars), it faithfully predicted the reduction in *Let-7b* observed in non-mutated HCC samples as well as the slightly larger decrease of *Let-7b* seen in HCC samples with *CTNNB1* mutation. The model also predicted the increased *LIN28B* expression in HCC which was similar whether *CTNNB1* was mutated or not (compare blue and white bars in Fig. 5A).

A second validation was obtained by considering previous results from a mouse model of MYC-induced liver cancer.[12] We simulated a 4,000-fold increase in *Myc* mRNA, which corresponds to the experimental induction of *Myc* in mice. Our simulation predicted a MYC-induced 7,000-fold overexpression of *Lin28b* mRNA and a 0.4-fold reduction in *Let-7b*. This prediction fitted well with the experimentally measured induction of *Lin28b* and reduction of *Let-7b* (Fig. 5B).

Third, as a proof of concept that the mathematical model can predict the impact of a pharmacological inhibitor of a GRN

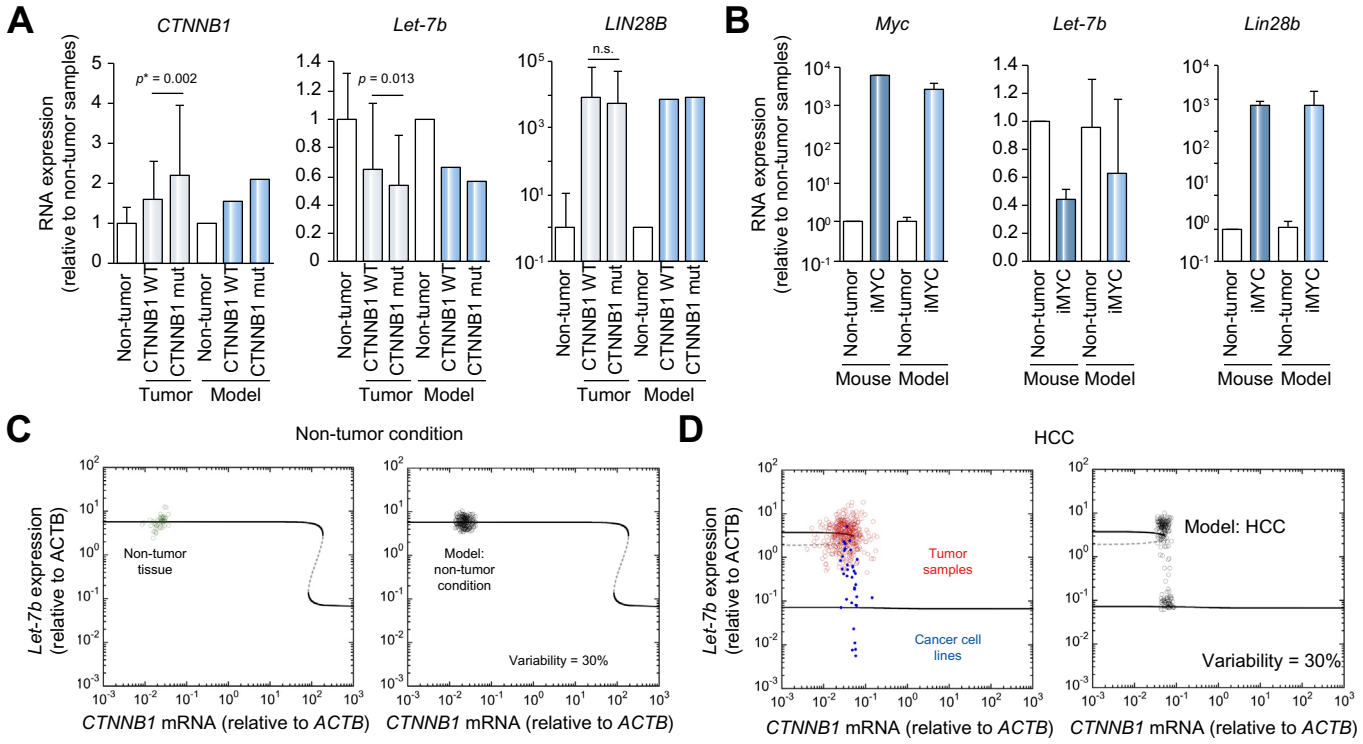

Fig. 5. Validation of the model and GRN dynamics in HCC. (A) Expression of stabilized CTNNB1 mutant (n = 98) and wild-type CTNNB1 (n = 270) in HCC compared to normal tissue (n = 50). The predicted levels of *Let-7b* and *LIN28* following a simulation of increased expression and stabilization of CTNNB1 fit with the experimental observations. (B) Measured and simulated impact of MYC induction on *LIN28B* mRNA and *Let-7b* expression levels, in a mouse model of MYC-induced HCC. (A, B) Results are means ± SD; *p* and *p** values calculated as in Fig. 1. (C) Modelling *Let-7b* levels as a function of *CTNNB1* mRNA in normal conditions (left). Values in non-tumor tissue (n = 50; green circles) are superimposed on the model curve. Solid curves, stable steady states; dashed curves, unstable steady states. Modelling 30% random variations around the basal value of each parameter in 200 cells resulted in a distribution of *Let-7b*/*CTNNB1* values in the upper stable state (right) which recapitulated the heterogeneity measured in normal samples. (D) Modelling *Let-7b*/*CTNNB1* mRNA values in HCC conditions (left). *Let-7b*/*CTNNB1* mRNA values in 368 HCC tumors (red circles) or 34 cell lines (blue dots) are superimposed on the model curve. Random variation of parameters like in (C) recapitulated the heterogeneity measured in patients with HCC and cell lines (right). See supplementary information for parameter values and numerical simulations. GRN, gene regulatory network; HCC, hepatocellular carcinoma. (This figure appears in colour on the web.)

component, we simulated the inhibition of LIN28B in HCC: simulating 60% inhibition of LIN28B protein predicted an increase in *Let-7b* and a decrease in SOX9 and MYC protein; CTNNB1 remained unaffected (Fig. 6). We then evaluated the results of the simulation in a HCC cell line, Huh7 (Fig. 6A), and in HCC31 primary liver cancer cells[17] (Fig. 6B), by growing these cells in the presence of LIN28 inhibitor (*N*-Methyl-*N*-[3-(3-methyl-1,2,4-triazolo[4,3-*b*]pyridazin-6-yl)phenyl]acetamide).[21] The inhibitor reduced cell proliferation (not shown), and, as expected, induced the expression of *Let-7b* and *Let-7a*. Importantly, the changes of SOX9, MYC and CTNNB1 protein levels measured by western blot matched well with the simulations (Fig. 6), thereby validating the mathematical model as a tool to predict the impact of a pharmacological inhibitor on the GRN.

GRN dynamics are characterized by a bistable switch

To characterize the dynamic properties of the GRN and determine whether they identify distinct HCC cell states, we modelled the steady-state levels of *Let-7b*, selected as a representative variable, as a function of *CTNNB1* mRNA. In normal conditions, high *Let-7b* was associated with low *CTNNB1* mRNA, and *vice versa* (Fig. 5C, left). The system exhibits a reversible bistable switch from high to low levels of Let-7b, at supraphysiological levels of *CTNNB1* mRNA. Green circles in Fig. 5C represent measured *Let-7b*/*CTNNB1* mRNA values in control samples from TGCA. However, simulating *Let-7b* as a function of *CTNNB1* mRNA in HCC conditions revealed an irreversible bistable switch occurring at low *CTNNB1* mRNA levels (Fig. 5D). Indeed, rising *CTNNB1* mRNA from low to supraphysiological levels in HCC would induce a switch from high to low *Let-7* expression, but reverting from supraphysiological *CTNNB1* to low *CTNNB1* levels would not allow high *Let-7* levels to be restored. The red circles in Fig. 5D reflect tumor-to-tumor heterogeneity of the HCCs and are predominantly positioned around the upper branch of the bistable switch. Blue dots in Fig. 5D represent *Let-7b*/*CTNNB1* values in 34 human HCC cell lines and reflect the cell line-to-cell line heterogeneity. These dots are predominantly positioned around the lower branch of the bistable switch, suggesting that culture conditions of cell lines promote switching of the GRN to a state distinct from the mean cell state in patient tumors. In non-tumor conditions (Fig. 5C), the expression of the GRN components is well below that of the threshold at which the bistable switch occurs. Therefore, a bistable switch is unlikely to contribute to the initiation of the disease. In contrast, in HCC, the expression level of GRN components in tumors and cell lines is around the threshold of the bistable switch, suggesting that the bistable switch can contribute to HCC progression (Fig. 5D).

The distribution of measured *Let-7b*/*CTNNB1* values in Fig. 5-C-D reflects inter-sample heterogeneity. When modelling a normal heterogeneous cell population with 30% of random variations around the basal value of each parameter, the

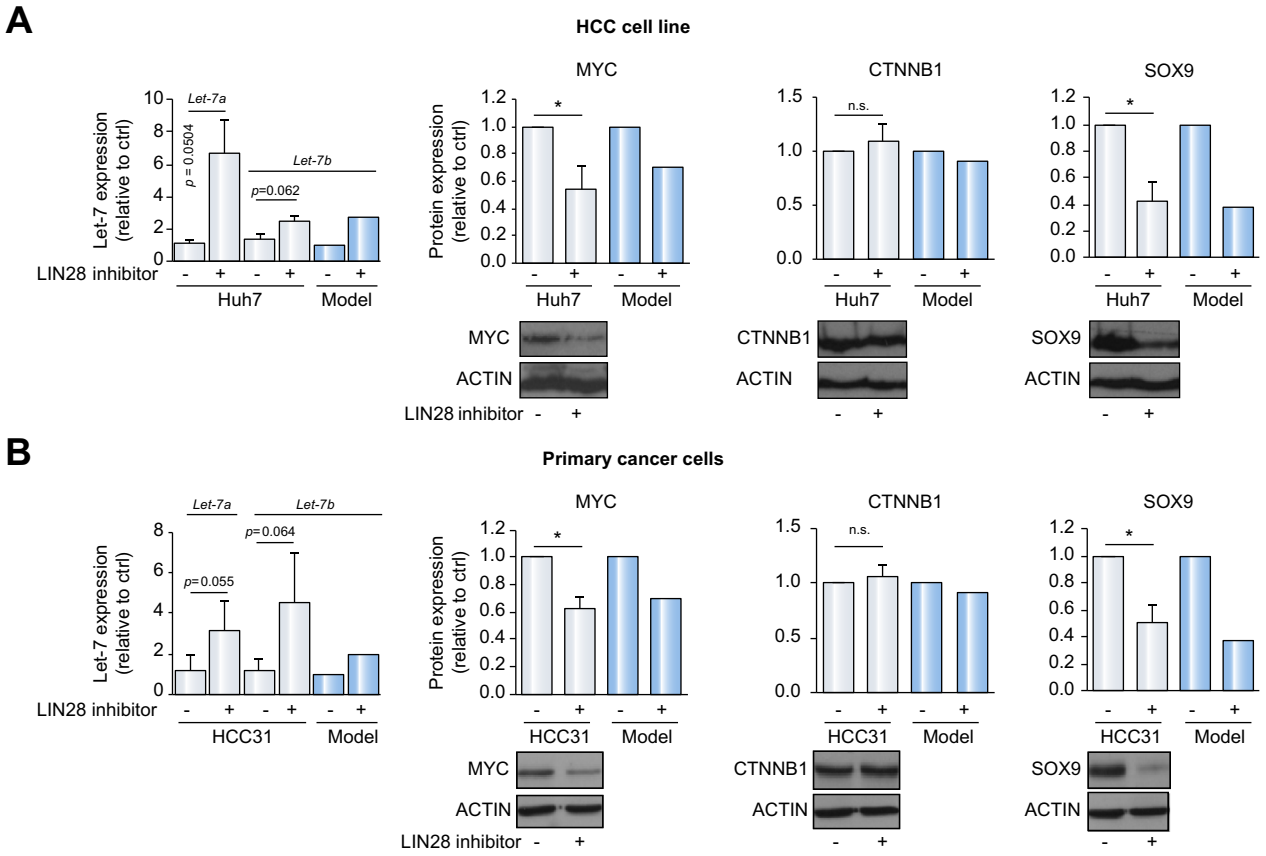

Fig. 6. Mathematical model as a tool to predict the impact of LIN28 inhibition on the GRN dynamics. (A, B) Simulating the absence (K_{ILET7} = 21) or presence (K_{ILET7} = 82) of LIN28 inhibition for 6 days (144 h) predicts expression levels of *Let-7b*, MYC, CTNNB1 and SOX9 which are close to the levels measured following (A) treatment of Huh7 cells and (B) HCC31 primary liver cancer cells with 120 μM of LIN28 inhibitor.[21] (B) *Let-7* expression levels were simulated and measured after 96 h. (A, B) Results are means ± SD; n ≥ 3; *$p < 0.05$ (Student's *t* test). GRN, gene regulatory network; HCC, hepatocellular carcinoma.

Let-7b|*CTNNB1* values remained clustered in the upper stable steady state (Fig. 5C, right). Modelling an HCC cell population with the same % of parameter variation generated a distribution of *Let-7b*|*CTNNB1* values similar to that seen in HCC patients and cell lines (Fig. 5D, right), indicating that the model accounts for the sample's heterogeneity.

We analyzed the robustness of the bistable switch dynamics in normal and HCC conditions towards variation in the value of different parameters (Fig. S6-7). These results showed that GRN dynamics rest on a robust reversible bistable switch that should not occur in normal conditions. Meanwhile, in HCC conditions, GRN dynamics exhibit a sensitive irreversible bistable switch that could cause heterogeneity among tumor samples.

GRN status in gastrointestinal cancers

We next verified if the GRN might be activated in cancers distinct from HCC. We looked at RNA expression in TCGA cohorts of cholangiocarcinoma, stomach and esophageal carcinoma, colorectal adenocarcinoma, thyroid carcinoma, kidney renal clear cell carcinoma, breast carcinoma, bladder urothelial carcinoma, and lung adenocarcinoma (Fig. 7A and Fig. S8). Significant and consistent induction of all tumor-promoting GRN components was detected in cholangiocarcinoma, stomach and esophageal carcinoma carcinoma, and colorectal adenocarcinoma, *i.e.* in gastrointestinal cancers. *Let-7b* did not show the expected reduction in those tumors, yet depending on the tumor type, other *Let-7* family members were downregulated, like in cholangiocarcinoma where *Let-7c* is strongly repressed. The other cancer types did not show a consistent increase in GRN components, suggesting that the GRN does not display tumor-promoting activity in these tumors.

Tu and coworkers developed a mouse model of colorectal cancer with a similar gene expression pattern as in human cancer,[22] which offered the opportunity to validate the mathematical model in this cancer type. The published mouse data showed that induction of *Lin28b* for 6 months triggered cell proliferation, downregulation of *Let-7* and upregulation of *Sox9*, the latter being illustrated by immunostaining.[22] The subsequent removal of *Lin28b* for 2 months partially restored the expression of *Let-7* and proliferation markers. As in the experiments,[22] the mathematical model predicted that a 6-month induction of *Lin28b* causes downregulation of *Let-7b* and upregulation of *Sox9*, and that those expression levels partially revert to near normal values 2 months after *LIN28* LIN28B removal (Fig. 7B), thereby validating the GRN model in colorectal cancer. The mathematical model also showed that the expression of *MYC* (Fig. 7B) and *CTNNB1* mRNAs (not shown) is not affected by *LIN28B* induction, which fitted well with the observations.[22]

Discussion

Here we identified a GRN which combines CTNNB1, SMARCA4, SOX9, LIN28B, Let-7b, TP53 and MYC. MYC expression is not strongly affected but it plays a role in mouse models of HCC.[12] Also, when comparing the HCC samples with low MYC expression with those expressing high levels of MYC, we found that

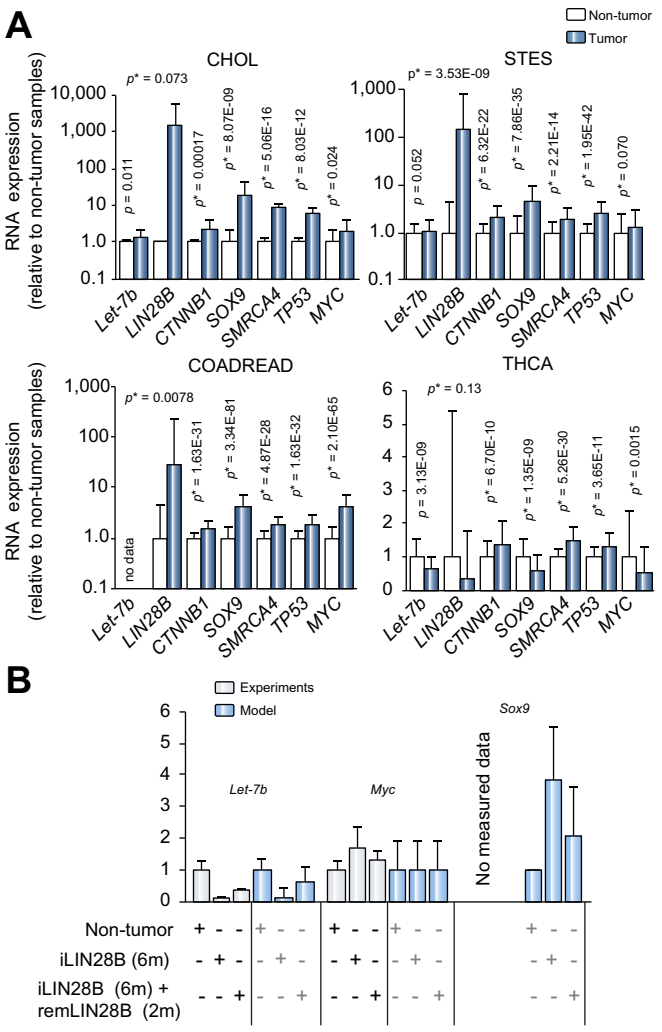

Fig. 7. Cancer-type specificity of GRN functionality and validation of the model in colorectal cancer. (A) Tumor-promoting components of the GRN are induced in CHOL, STES, and COADREAD. THCA had a distinct gene expression profile. Data (mean ± SD) are from TCGA; the number of normal and tumor samples is 9 and 36 (CHOL), 50 and 600 (STES), 51 and 624 (COADREAD), and 59 and 501 (THCA). (B) RNA levels of *Let-7b*, *Myc* and *Sox9* in experiment (grey) and in the model (blue) in non-tumor condition, after 6 months of *Lin28b* induction (LIN28B), and after 6 months of *Lin28b* induction followed by 2 months of partial *Lin28b* removal (remLIN28B) (see supplementary information for parameter values). CHOL, cholangiocarcinoma; COADREAD, colorectal adenocarcinoma; GRN, gene regulatory network; STES, stomach and esophageal carcinoma; TCGA, The Cancer Genome Atlas; THCA, thyroid carcinoma. *p* and *p** values calculated as in Fig. 1.

MYC expression positively correlates with nearly all GRN components, namely CTNNB1, SOX9, SMARCA4 and TP53 (Fig. S2).

Since the mathematical model resorts to 2 sets of parameters, one for normal conditions and one for tumors and cell lines, it accounts for the GRN dynamics in each state, but not for the dynamical transition between normal and HCC states. Indeed, to properly calibrate the model on mRNA expression, the transcription rates of *LIN28B*, *SOX9*, mutant *TP53*, *CTNNB1* and *SMARCA4* had to be increased in the HCC conditions ('*tumor*' parameter in Tables S4-5). This indicates that the interactions between GRN components are not sufficient to account for the normal-to-HCC transition. The parameters implicitly integrate the impact of external regulators of the GRN. Yet, the modelling strategy cannot integrate the full spectrum of regulations, and a number of regulators might not be known. Since modelling the transition from normal to HCC requires adaptation of the transcription rates of *LIN28B*, *SOX9*, mutant *TP53*, *CTNNB1* and *SMARCA4*, we suggest that the mechanisms controlling the expression of those genes warrant further investigation.

Classifying HCCs identified proliferative versus non-proliferative classes, or subdivided patients with HCC into subgroups G1 to G6.[19] Consistently, the GRN is most activated in the G1, G2 and G3 subgroups which are associated with poor differentiation, severe prognosis, and overexpression of genes regulating cell proliferation.[19] The targets of CTNNB1 are heterogeneous as CTNNB1 induces progenitor-type genes in tumor cells such as cyclin-D1 or VEGF-A, but also regulates expression of antioxidant, pro-survival and pro-hepatocyte differentiation genes in normal hepatocytes.[23] The G5 and G6 subgroups are associated with activation of CTNNB1 targets typical of mature hepatocytes, whereas the G1, G2, and G3 subgroups show predominant activation of progenitor-type targets. Interestingly, high GRN status was associated with high expression of progenitor-type CTNNB1/TCF/LEF targets (Fig. S9 and Table S8). *TERT* promoter mutations are found in 60% of HCCs.[13,24] However, out of the 368 HCC samples of the TCGA cohort, the 100 samples with the highest *TERT* expression did not consistently misexpress GRN components compared to the 268 HCC samples with lower *TERT* expression levels (Fig. S9C).

The GRN comprises positive feedback loops which are at the origin of bistable switches. To our knowledge, our work identified the first potential irreversible bistable switch involved in a specific subset of HCC tumors. The identification of irreversible states in HCC provides evidence that targeting specific GRN components using drugs might be therapeutically ineffective when cancer cells are in a locked state with regard to the function of the drug target. Also, our comparison of patient tumors and cultured HCC lines indicates that cell lines may be in a state distinct from that of tumors with regard to the function of the GRN.

To facilitate the analysis of the GRN, we set up a web-platform allowing researchers to check the GRN status in new samples of HCC and gastrointestinal tumors. This platform presents a graphical user interface that integrates the expression levels of the GRN components of tumor samples, and which implements the mathematical model to test which component of the network is the best target to modulate the network dynamics (http://biomodelling.eu/apps.html).

In conclusion, we anticipate that identification and dynamical modelling of a set of GRNs composed of interacting components that are often mutated and/or dysregulated in HCC, as is the case here for CTNNB1 and *Let-7*/LIN28,[6,10,12,25] will contribute to provide a global picture of tumor-promoting gene function in HCC. Our study presents a concept and tools that could help in the design of bespoke therapies for the treatment of HCC.

Financial support

The work of FPL was supported by the Interuniversity Attraction Pole Programme (Belgian Science Policy, PVII-47), the D.G. Higher Education and Scientific Research of the French Community of Belgium (ARC 15/20-065), the F.R.S.-FNRS (Belgium: Grants T.007214 and J.0058.15), and the Belgian Foundation Against Cancer (grant 2014-125). J.Z-R's group is supported by INSERM (France), the Ligue Nationale contre le Cancer (France, Equipe Labellisée), Labex OncoImmunology (France, investissement d'avenir), Coup d'Elan de la Fondation Bettencourt-

Shueller (France), the SIRIC CARPEM (France) and Fondation Mérieux (France). J.U.M. is supported by grants from the German Research Foundation (MA 4443/2-2) and the Volkswagen Foundation (Germany, Lichtenberg program).

Conflict of interest

The authors declare no conflicts of interest that pertain to this work.

Please refer to the accompanying ICMJE disclosure forms for further details.

Authors' contributions

C.G. and F.P.L. conceived and designed the study. C.G. performed transcriptomic data analysis and mathematical modelling. M.D-L., K.K. and S. Cordi performed transfection experiments and quantified RNA and proteins. L.G. created the web-based platform under supervision of E.H. A.L. did the survival analysis and helped with transcriptomic data analysis. S. Caruso, G.C. and J.Z-R. provided transcriptomic data and human cell lines and contributed to the interpretation of the modelling results. D.C. and J.U.M. provided primary human HCC cells. J.T. and S. P.M. shared and analysed data from transgenic mice. C.G., M. D-L. and F.P.L. wrote the manuscript with input from all authors.

Acknowledgements

The authors thank P. Jacquemin, C. Pierreux, L. Desmet and the Lemaigre laboratory members for help, and L. Nguyen and H. Zhu for sharing information.

Supplementary data

Supplementary data to this article can be found online at https://doi.org/10.1016/j.jhep.2019.03.024.

References

Author names in bold designate shared co-first authorship

[1] Calderaro J, Couchy G, Imbeaud S, Amaddeo G, Letouze E, Blanc JF, et al. Histological subtypes of hepatocellular carcinoma are related to gene mutations and molecular tumour classification. J Hepatol 2017;67:727–738.

[2] Uhlen M, Zhang C, Lee S, Sjostedt E, Fagerberg L, Bidkhori G, et al. A pathology atlas of the human cancer transcriptome. Science 2017;357, pii: eaan2507.

[3] **Schulze K**, **Imbeaud S**, **Letouze E**, Alexandrov LB, Calderaro J, Rebouissou S, et al. Exome sequencing of hepatocellular carcinomas identifies new mutational signatures and potential therapeutic targets. Nat Genet 2015;47:505–511.

[4] Cancer Genome Atlas Research Network. Comprehensive and Integrative Genomic Characterization of Hepatocellular Carcinoma. Cell 2017;169, 1327–1341 e1323.

[5] Breuhahn K, Gores G, Schirmacher P. Strategies for hepatocellular carcinoma therapy and diagnostics: lessons learned from high throughput and profiling approaches. Hepatology 2011;53:2112–2121.

[6] Tao J, Zhang R, Singh S, Poddar M, Xu E, Oertel M, et al. Targeting beta-catenin in hepatocellular cancers induced by coexpression of mutant beta-catenin and K-Ras in mice. Hepatology 2017;65:1581–1599.

[7] **Zeng X**, **Lin Y**, **Yin C**, Zhang X, Ning BF, Zhang Q, et al. Recombinant adenovirus carrying the hepatocyte nuclear factor-1alpha gene inhibits hepatocellular carcinoma xenograft growth in mice. Hepatology 2011;54:2036–2047.

[8] Thorgeirsson SS, Grisham JW. Molecular pathogenesis of human hepatocellular carcinoma. Nat Genet 2002;31:339–346.

[9] **Jung KH**, **Zhang J**, Zhou C, Shen H, Gagea M, Rodriguez-Aguayo C, et al. Differentiation therapy for hepatocellular carcinoma: Multifaceted effects of miR-148a on tumor growth and phenotype and liver fibrosis. Hepatology 2016;63:864–879.

[10] Takashima Y, Terada M, Udono M, Miura S, Yamamoto J, Suzuki A. Suppression of lethal-7b and miR-125a/b maturation by Lin28b enables maintenance of stem cell properties in hepatoblasts. Hepatology 2016;64:245–260.

[11] Viswanathan SR, Powers JT, Einhorn W, Hoshida Y, Ng TL, Toffanin S, et al. Lin28 promotes transformation and is associated with advanced human malignancies. Nat Genet 2009;41:843–848.

[12] **Nguyen LH**, **Robinton DA**, **Seligson MT**, Wu L, Li L, Rakheja D, et al. Lin28b is sufficient to drive liver cancer and necessary for its maintenance in murine models. Cancer Cell 2014;26:248–261.

[13] Zucman-Rossi J, Villanueva A, Nault JC, Llovet JM. Genetic landscape and biomarkers of hepatocellular carcinoma. Gastroenterology 2015;149, 1226–1239 e1224.

[14] Wilkinson AC, Nakauchi H, Gottgens B. Mammalian transcription factor networks: recent advances in interrogating biological complexity. Cell Syst 2017;5:319–331.

[15] **Rata S**, **Suarez Peredo Rodriguez MF**, Joseph S, Peter N, Echegaray Iturra F, Yang F, et al. Two interlinked bistable switches govern mitotic control in mammalian cells. Curr Biol 2018;28, 3824–3832 e3826.

[16] Ryu H, Chung M, Dobrzynski M, Fey D, Blum Y, Lee SS, et al. Frequency modulation of ERK activation dynamics rewires cell fate. Mol Syst Biol 2015;11:838.

[17] Castven D, Becker D, Czauderna C, Wilhelm D, Andersen JB, Strand S, et al. Application of patient-derived liver cancer cells for phenotypic characterization and therapeutic target identification. Int J Cancer 2019;144:2782–2794.

[18] Kaposi-Novak P, Lee JS, Gomez-Quiroz L, Coulouarn C, Factor VM, Thorgeirsson SS. Met-regulated expression signature defines a subset of human hepatocellular carcinomas with poor prognosis and aggressive phenotype. J Clin Invest 2006;116:1582–1595.

[19] **Boyault S**, **Rickman DS**, **de Reynies A**, Balabaud C, Rebouissou S, Jeannot E, et al. Transcriptome classification of HCC is related to gene alterations and to new therapeutic targets. Hepatology 2007;45:42–52.

[20] Rebouissou S, La Bella T, Rekik S, Imbeaud S, Calatayud AL, Rohr-Udilova N, et al. Proliferation markers are associated with MET expression in hepatocellular carcinoma and predict tivantinib sensitivity in vitro. Clin Cancer Res 2017;23:4364–4375.

[21] **Roos M**, **Pradere U**, Ngondo RP, Behera A, Allegrini S, Civenni G, et al. A small-molecule inhibitor of Lin28. ACS Chem Biol 2016;11:2773–2781.

[22] Tu HC, Schwitalla S, Qian Z, LaPier GS, Yermalovich A, Ku YC, et al. LIN28 cooperates with WNT signaling to drive invasive intestinal and colorectal adenocarcinoma in mice and humans. Genes Dev 2015;29: 1074–1086.

[23] Nejak-Bowen KN, Monga SP. Beta-catenin signaling, liver regeneration and hepatocellular cancer: sorting the good from the bad. Semin Cancer Biol 2011;21:44–58.

[24] Nault JC, Mallet M, Pilati C, Calderaro J, Bioulac-Sage P, Laurent C, et al. High frequency of telomerase reverse-transcriptase promoter somatic mutations in hepatocellular carcinoma and preneoplastic lesions. Nat Commun 2013;4:2218.

[25] **Wu L**, **Nguyen LH**, Zhou K, de Soysa TY, Li L, Miller JB, et al. Precise let-7 expression levels balance organ regeneration against tumor suppression. Elife 2015;4 e09431.